

See discussions, stats, and author profiles for this publication at: <https://www.researchgate.net/publication/271769760>

# Electromechanical Signatures for DNA Sequencing through a Mechanosensitive Nanopore

ARTICLE *in* JOURNAL OF PHYSICAL CHEMISTRY LETTERS · JANUARY 2015

Impact Factor: 7.46 · DOI: 10.1021/jz5025417

---

CITATIONS

2

---

READS

295

## 3 AUTHORS, INCLUDING:



Amir Barati Farimani  
Stanford University  
21 PUBLICATIONS 135 CITATIONS

[SEE PROFILE](#)

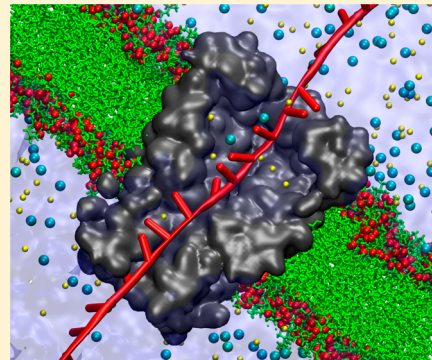
## Electromechanical Signatures for DNA Sequencing through a Mechanosensitive Nanopore

A. Barati Farimani,<sup>†</sup> M. Heiranian,<sup>†</sup> and N. R. Aluru\*

Department of Mechanical Science and Engineering, Beckman Institute for Advanced Science and Technology, University of Illinois at Urbana-Champaign, Urbana, Illinois 61801, United States

 Supporting Information

**ABSTRACT:** Biological nanopores have been extensively used for DNA base detection since these pores are widely available and tunable through mutations. Distinguishing bases of nucleic acids by passing them through nanopores has so far primarily relied on electrical signals—specifically, ionic currents through the nanopores. However, the low signal-to-noise ratio makes detection of ionic currents difficult. In this study, we show that the initially closed mechanosensitive channel of large conductance (MscL) protein pore opens for single-stranded DNA (ssDNA) translocation under an applied electric field. As each nucleotide translocates through the pore, a unique mechanical signal is observed—specifically, the tension in the membrane containing the MscL pore is different for each nucleotide. In addition to the membrane tension, we found that the ionic current is also different for the four nucleotide types. The initially closed MscL adapts its opening for nucleotide translocation due to the flexibility of the pore. This unique operation of MscL provides single nucleotide resolution in both electrical and mechanical signals. Finally, we also show that the speed of DNA translocation is roughly 1 order of magnitude slower in MscL compared to *Mycobacterium smegmatis* porin A (MspA), suggesting MscL to be an attractive protein pore for DNA sequencing.



Nanopore-based DNA sequencing is attractive as it is a label-free, single-molecule approach that can be utilized for high-precision DNA analysis.<sup>1–3</sup> Biological nanopores have been investigated for DNA base detection since they offer several advantages for single-molecule DNA analysis.<sup>2–8</sup> First, mutagenesis can be used to tailor the physical and chemical properties of biological nanopores;<sup>1,8</sup> Second, biological nanopores are synthesized by cells with an atomic level precision that may not be possible with solid-state fabrication approaches;<sup>9</sup> Third, crystallography data of protein channels is available at angstrom length scales.<sup>1,2,4,9</sup> The first biological nanopore investigated for sequencing DNA was staphylococcal  $\alpha$ -hemolysin ( $\alpha$ HL) protein pore;<sup>10</sup> an applied potential translocated a single-stranded DNA (ssDNA) molecule through the pore giving rise to modulation of the ionic current.<sup>5</sup>  $\alpha$ HL cylindrical  $\beta$  barrel (with a diameter of 2 nm and length of 5 nm) is not tight enough to yield a distinguishable ionic current specific to individual nucleotides and therefore, exhibits small current differences between the nucleotides. Another well-researched biological nanopore for DNA sequencing is *Mycobacterium smegmatis* porin A (MspA).<sup>11,12</sup> MspA has been shown to provide better ionic current signals for differentiating nucleotides as its pore structure includes a tighter 1.2 nm constriction region.<sup>12</sup> In contrast to synthetic nanopores, such as graphene<sup>13–15</sup> and MoS<sub>2</sub> nanopores<sup>16,17</sup> where DNA base could be electronically read through transverse tunneling current,<sup>18–20</sup> ionic current is the only signature that has been acquired in biological nanopores, e.g., in MspA or  $\alpha$ HL. The noise in the system and the presence of

multiple bases in these nanopores make detection of a single DNA base difficult.<sup>1</sup> Acquiring another signal, in addition to ionic currents, for DNA detection using biological pores can significantly increase the accuracy of DNA sequencing.

The sensing of mechanical tension and force within a cell's environment is mostly mediated by a highly specialized class of membrane proteins known as mechanosensitive (MS) ion channels.<sup>12</sup> MS channels were shown to be able to transduce mechanical tension into an electrochemical response.<sup>21</sup> When a cell membrane is under tension due to osmotic down shock, MS channels relieve the pressure of the cell by gating and forming a pore as big as 3 nm in diameter.<sup>22,23</sup> Among several types of MS channels, the mechanosensitive channel of large conductance (MscL) of prokaryotes has been most extensively characterized.<sup>22,24–29</sup>

Here, we demonstrate for the first time that a MscL nanopore can be used for detection of DNA bases by modulating tension and strain in MscL. Tension in the MscL membrane, along with the ionic currents, can be used for more precise sequencing of DNA (see the cartoon representation of the system in Figure 1a). Unlike  $\alpha$ HL or MspA, which are structurally wide open pores, the initially closed MscL pore opens as an ssDNA translocates through the pore due to an applied electric field. MscL adjusts its pore size to the size of

Received: December 2, 2014

Accepted: January 28, 2015



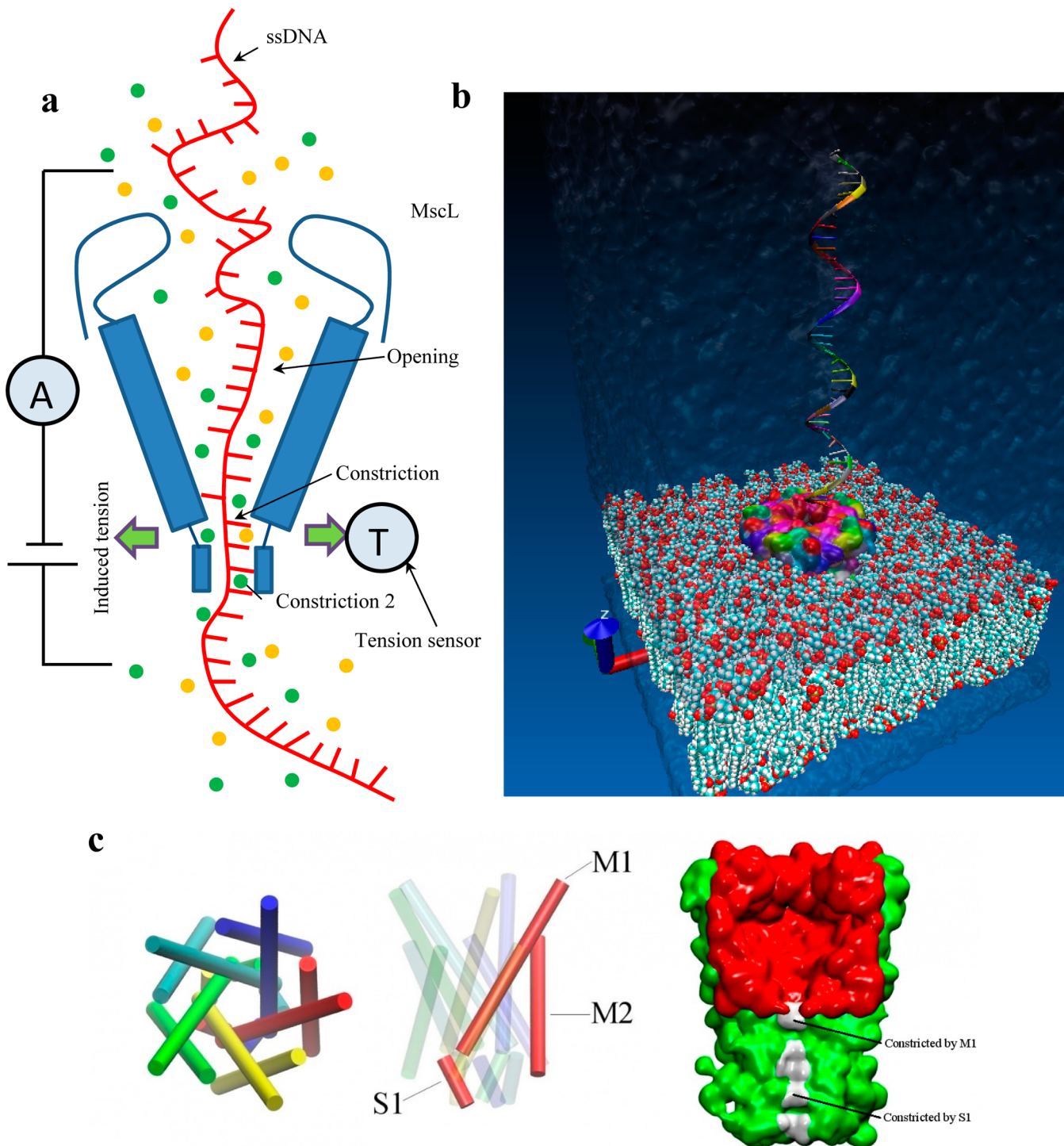


**Figure 1.** (a) Cartoon representation of the system (MscL, ssDNA, ions) demonstrating two parallel signals: tension and ionic current. (b) Visualization of the simulation setup comprising ssDNA, MscL protein, lipid bilayer and water. (c) Left: Top view of MscL. Middle: side view of MscL with the designation of M1 and M2 helices. Right: Pore architecture of MscL, cut in the middle and the location of the two constriction regions of MscL. (d) Force (averaged) induced in the membrane due to the presence of each base in MscL.

DNA bases during the translocation. The distinct tension in the protein associated with each nucleotide can be sensed through the strain and tension induced in the lipid bilayer. Recently,<sup>30</sup> MscL has been successfully embedded and characterized inside a droplet interface bilayer (DIB). It has been shown that the induced tension inside MscL is translated into a change in the triple point angle of DIB. By monitoring the angle change in

DIB during DNA translocation, induced tension can be measured and quantified.

Two well-known challenges of DNA detection through nanopores are the fast translocation speed of DNA and noise.<sup>1,2,9</sup> Experiments have shown that DNA passes through  $\alpha$ HL with a speed of  $1\text{base}/\mu\text{s}$ , requiring MHz signal measurements to differentiate between nucleotide types.<sup>1,2</sup> The presence of multiple bases in the pore and thermal

fluctuations in the system generate noise in the ionic current, making detection difficult. A MscL nanopore is flexible<sup>31</sup> and it adjusts to DNA size, causing a reduction in the speed of translocation. We demonstrate the slower translocation of DNA in MscL by comparing the results in MspA nanopore. Furthermore, we demonstrate the effect of pore flexibility by comparing the results in MscL and MspA pores.

We performed molecular dynamics (MD) simulations with NAMD 2.6 using the Petascale Blue Waters machine.<sup>32</sup> A typical simulation set up consisting of ssDNA, MscL protein, lipid bilayer, water and ions (~600,000 atoms) is shown in Figure 1b (see Supporting Information Movie 1). We used the closed MscL model provided by Sukharev et al., and the crystal structure was obtained from Chang et al.<sup>12,21</sup> The  $\text{C}\alpha$  segments were eliminated to obtain a reduced version of MscL.<sup>12,21</sup> A lipid bilayer (1-palmitoyl-2-oleoyl-sn-glycero-3-phosphocholine (POPC)) patch was created ( $10 \text{ nm} \times 10 \text{ nm}$ ) to accommodate the protein and solvated by a 25-Å thick slab of water on each side of the membrane. MscL with the center of the pore aligned along the membrane normal axis ( $z$ -axis) was placed in the lipid bilayer using Visual Molecular Dynamics (VMD).<sup>33</sup> We ran the simulation for 40 ns to equilibrate the system of lipid bilayer and protein. This long equilibration makes sure that the protein is firmly placed in the membrane without any membrane leakage. Using the equilibrated lipid–protein system, ssDNA was placed at the mouth of the MscL nanopore with the ssDNA axis ( $z$ -direction) aligned along the protein axis (Figure 1b). Then, ssDNA (one at a time), MscL, and the lipid bilayer were submersed in water and salt ionic solution. The ionic concentration of NaCl was 0.5 M. We used polydA(60), polydC(60), polydT(60) and polydG(60) to create four simulation boxes (Figure 1b) differing only in ssDNA type. We used the CHARMM27 force field<sup>34</sup> parameters for the protein, nucleic acid (DNA), TIP3P water molecules, and ions. SHAKE algorithm was used to maintain the rigidity of the water molecules. Periodic boundary condition was applied in all the three directions. The cut-off distance for the LJ interactions was 15 Å. The long-range electrostatic interactions were computed by using the particle-mesh-Ewald (PME) method. The time step was selected to be 1 fs. For each simulation, energy minimization was performed for 100 000 steps. The system was then equilibrated for 5 ns with NPT ensemble at 1 atm pressure and 300 K temperature. NPT simulation ensures that the water concentration is equal to the bulk value of 1 g/cm<sup>3</sup>. The simulation was then performed in NVT ensemble. Temperature was maintained at 300 K by applying the Nosé–Hoover thermostat with a time constant of 0.1 ps. Before applying the electric field, equilibration for 2 ns was performed in NVT. Production simulations were performed by applying an external electric field in the  $z$ -direction. The external electric fields are reported in terms of a transmembrane voltage difference  $V = EL_z$ , where  $E$  is the electric field strength and  $L_z$  is the length of the simulation system in the  $z$ -direction.<sup>14</sup> For computational efficiency, we used steered molecular dynamics (SMD) to pull DNA with a very slow velocity of 0.00001 Å/fs. The steering forces were applied to all the atoms (both charged and uncharged) of the first base entering the pore. We monitored the time-dependent ionic current,  $I(t)$ , in the pore. We computed the ionic current through the nanopore by using the definition of current,  $I = dq/dt$ , as  $I(t) = 1/L_z \sum_{i=1}^n q_i [(z_i(t + \delta t) - z_i(t))/(\delta t)]$ , where the sum is for all the ions,  $\delta t$  is chosen to be 5 ps, and  $z_i$  and  $q_i$  are the  $z$ -coordinate and charge of ion  $i$ , and  $n$  is the total number

of ions. The ionic current data is averaged for each base, and the average current per base was reported.

To characterize the tension in the protein due to nucleotide translocation, the interaction forces between MscL helices and DNA bases were calculated. Subunits of MscL containing M1, M2, and S1 helices are shown in different colors in Figure 1c. Since MscL has five identical subunits, pair interaction calculations were carried out separately for each subunit. Both Coulombic and vdW (van der Waals) forces by DNA bases on the inner transmembrane helix (M1) and the S1 helix (Figure 1c) were computed every picosecond and then averaged over the entire DNA translocation time for each subunit of MscL. Only the inner M1 and S1 helices that create the constriction regions (Figure 1c) inside MscL were considered, and the outer helices (M2) were ignored. The radial components of the calculated forces directed away from the center of the protein channel were then spatially averaged over all the five identical subunits of MscL to obtain an average force per subunit corresponding to each DNA base type. The nature of these forces is tensile and, therefore, the induced tension in MscL is transferred to the membrane since its segments are radially pushed outward by ssDNA. We refer to these interaction forces between ssDNA and protein lining residues as tension. It is notable that the origin of this tension is different from the tension defined as the membrane tension that causes MscL to gate.

We found four different tension signals for bases A, C, G, and T which can be used for detecting and discriminating between nucleotides (Figure 1d). We observed that the maximum induced force is from base T, and the order of the induced forces is T > G > C > A. The force between ssDNA and MscL is from vdW and electrostatic interactions. Prior work has shown that a 70 pN force can open the MscL protein channel, therefore the range of 20–120 pN forces induced from translocation of different bases should be adequate for the discrimination of bases.<sup>23,28</sup> Also, using magnetic tweezers, it is possible to measure forces as small as 50 fN,<sup>35</sup> therefore forces of 20 pN magnitude should be measurable. These forces on the wall of the protein channel have a local effect on the lipid bilayer. The effect of the forces and tension is maximum on the lipids in the vicinity of MscL, therefore the force measurements need to be done on the lipids, close to the protein. To understand why base T induces a maximum force, we investigated the structure and interaction parameters of each base. Base T has two protruding oxygen atoms, and this is the maximum number among all the bases (more information about the structure of bases and their interaction strength can be found in the Supporting Information). Oxygen plays a significant role in both vdW and electrostatic forces between MscL lumen lining residues and nucleotides. The Lennard-Jones (LJ) energy interaction parameter of the oxygen atom is higher ( $\epsilon_O = 0.210$ ) compared to all the other atoms ( $\epsilon_H = 0.05$ ,  $\epsilon_C = 0.1$ ,  $\epsilon_N = 0.17$ )<sup>36</sup> of the base. Base A has only hydrogen terminations (no oxygen), therefore it has the lowest interactive forces among all the bases (Figure 1d). Comparing the termination structure of bases G and C reveals the existence of two nitrogens and one oxygen for base G, and only one nitrogen and oxygen for base C. The extra nitrogen in base G compared to base C gives rise to the higher interaction forces between MscL and base G, and this fact explains the interaction forces order (G > C).

Unlike other biological pores (MspA or  $\alpha$ HL) and solid-state nanopores, which are normally open, MscL has a flexible pore

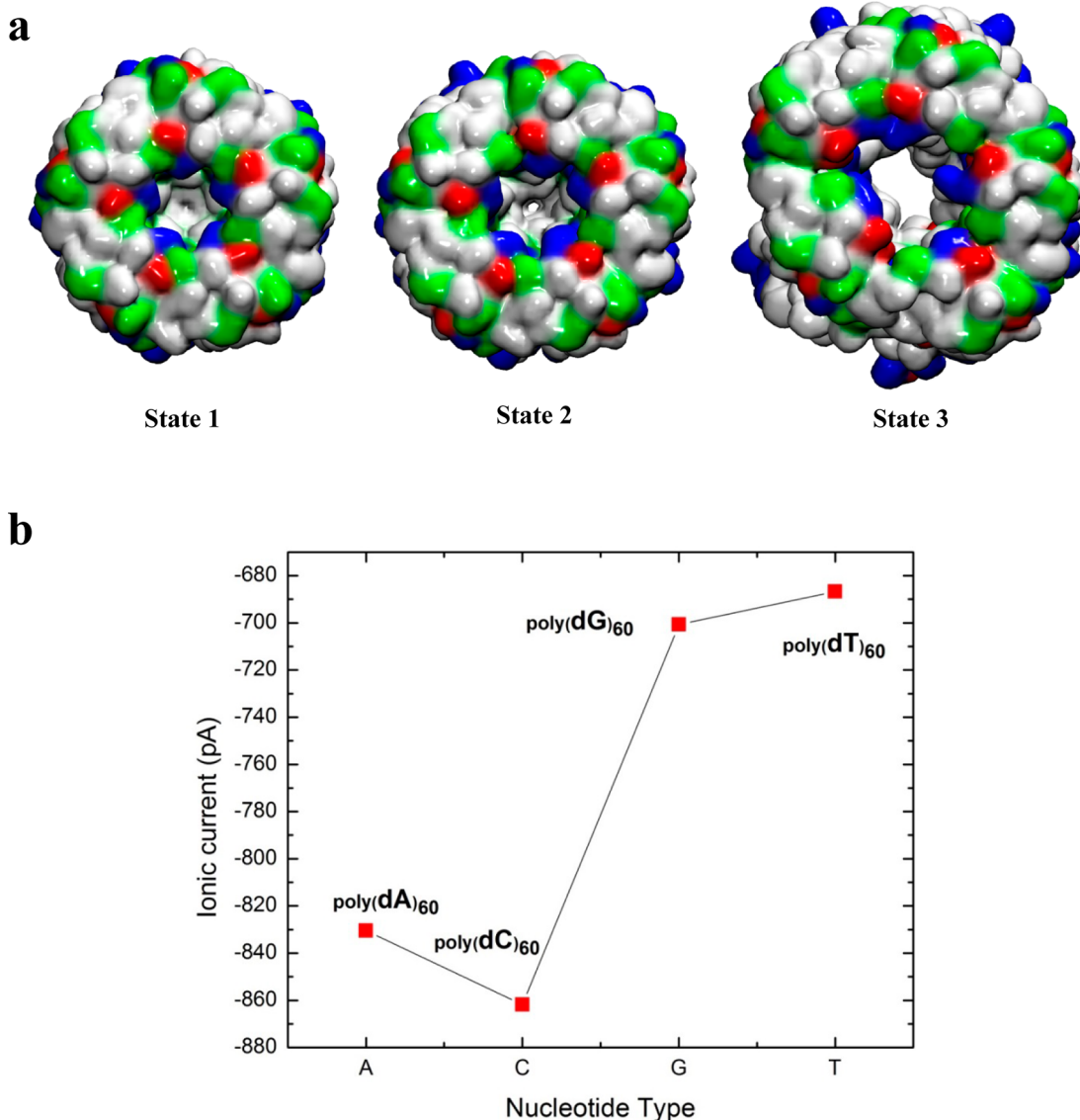


**Figure 2.** (a) Three representative states of the MscL pore and the extent to which it opens. State 1: initially closed state prior to the ssDNA entry; State 2: the first base of ssDNA entered the pore and is about to exit the cytoplasmic segment of the pore (the pore opens partially); State 3: ssDNA with 60 bases (here, polydA) translocated and pore has an elliptical shape. (b) Average ionic current for different nucleotide types.

as it opens according to the size of the base, i.e., in our simulations, initially, MscL opens with evolving pore radii during the translocation of the first 5–10 bases (see Supporting Information Movie 2). In the calculation of forces, we ignored the force data from the initial entry of ssDNA (for all PolydA, PolydC, PolydG and PolydT) into MscL, because these forces are not in equilibrium and the pore exhibits transient dynamics. In Figure 2a (see also Supporting Information Movie 2), we show three states of the pore representing the pore opening and expansion. State 1, state 2, and state 3 refer to closed, transient opening (while the first bases of PolydA are about to exit the cytoplasmic segment of MscL), and fully opened by polydA states, respectively. Interestingly, the MscL pore has an elliptical shape when it is fully open (Figure 2a). It is notable that in normal operation of MscL, in both intermediate and open states, the MscL pore is circular and symmetrical (see Supporting Information Movie 3).

We computed the average ionic current for each base (averaged during the translocation of each polydna with 60

bases) and found the current to decrease in the order, C > A > G > T. The ionic currents of bases C and A are close to each other and higher compared to bases G and T. Most of the ions that passed through the pore are cations which are dragged by the negatively charged backbone of the DNA during the translocation of all the 60 bases. A very small number of ions are trapped between the bases and dragged down the pore. Water molecules are observed in the pore all around the DNA. To illustrate the effect of pore elasticity of MscL on the quality of the acquired ionic current signal, we compared the ionic current signals for both MscL and MspA nanopores (Supporting Information). According to the literature, MspA has been found to be the best biological pore, reported so far, for DNA detection.<sup>2,11,37,38</sup> The maximum and minimum current difference,  $\Delta I$ , is 113.1 pA and 189.2 pA for MspA and MscL, respectively (Supporting Information). Higher  $\Delta I$  for MscL compared to MspA shows a better detection signal for MscL. We also investigated the noise by computing the signal-to-noise ratio, SNR, for both MscL and MspA pores. SNR is

6.13 (with  $I_{\text{noise,RMS}} = 30.99 \text{ pA}$ ) and 4.21 (with  $I_{\text{noise,RMS}} = 26.84 \text{ pA}$ ) for MscL and MspA, respectively (Supporting Information). To compare the noise for static and moving ssDNA, we performed simulation of moving ssDNA by applying bias (500 mV) and static ssDNA when ssDNA is inside MscL and the applied bias is zero. We used the same method of noise calculation that we used in SNR computation (Supporting Information). The ratio of noise generated in the static ssDNA case ( $I_{\text{noise,RMS:Static}}$ ) and noise generated in moving ssDNA case ( $I_{\text{noise,RMS:Moving}}$ ), is  $I_{\text{noise RMS:Static}}/I_{\text{noise RMS:Moving}} = 0.985$ , which means the noise is very similar in both cases. The signal becomes strong (or the SNR is improved) when a strong bias (no SMD) is applied leading to a high DNA passage rate. Therefore, DNA translocation rate is indirectly related to the strength of the signal and consequently the signal-to-noise ratio.

The fluctuations in current are dependent on the slit diameter, slit length, and the charged lining residues of the slit. In MscL, the diameter of the pore is flexible and adaptive to the ssDNA nucleotide type. We believe this flexibility, and perhaps selectivity, reduces the noise level, as noted in the SNR comparison of MspA and MscL. The distinctive ionic current features in MscL can be attributed to two fundamental differences between the operation of MscL and other biological nanopores. First, in MscL, the pore is initially closed, and it opens due to the electric field-mediated translocation of ssDNA, unlike in other nanopores where a fixed pore diameter is employed. Second, unlike MspA,  $\alpha$ -HL,  $\text{Si}_3\text{N}_4$ , graphene, and  $\text{MoS}_2$ , MscL has two constriction regions that open during ssDNA translocation (see Figure 1c). Bases C and A have larger ionic currents (Figure 2b), revealing the fact that these bases are capable of transporting ions through the constriction regions with higher rates. To understand how the MscL pore opens during the translocation of bases, we time-averaged the pore radius during ssDNA translocation (Figure 3a). Base A creates the largest pore diameter, and base T creates the smallest pore diameter in constriction 1, constriction 2, and open regions of the MscL channel (Figure 3a). The minimum ionic current is for base T (Figure 2b), and this is consistent with the minimum opening of the pore induced by base T in all the segments of MscL (Figure 3a). The order of pore radii opened by ssDNA in constriction regions 1 and 2 and the open region is A > G > C > T. Bases A and G (purines) have an additional ring compared to bases C and T (pyrimidines), which gives rise to the larger base area of purines and the consequent larger pore radii in MscL compared to pyrimidines (Supporting Information).

The normal activation of MscL by tension in the lipid bilayer has two open states: intermediate and fully open. In the closed state, the S1 segments form a bundle, and the cross-linking of S1 segments prevents the opening of the channel (Figure 1c). When tension is applied to the membrane, the transmembrane barrel-like structure expands and stretches apart the S1-M1 region, allowing the channel to open (Figure 1c). The transition from the closed to the intermediate state includes small movements of the M1 helix. Further transitions to the open states are characterized by large movements in both M1 and M2. The gating pathway for ssDNA translocation through MscL is, however, different. We compared the conformational changes occurring in the pore lumen due to ssDNA translocation with the normal operation of MscL (Figure 3b). The average pore radii for the three stable structures of MscL and ssDNA-opened MscL are shown in Figure 3b. The

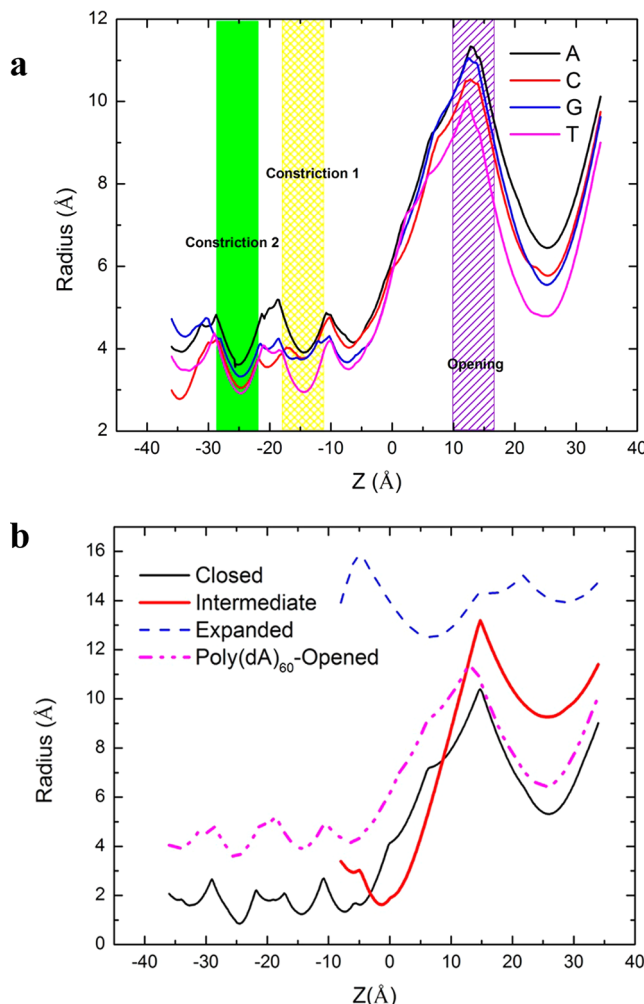


**Figure 3.** (a) Average pore radius of MscL during translocation of Poly(dA)<sub>60</sub>, Poly(dC)<sub>60</sub>, Poly(dG)<sub>60</sub>, and Poly(dT)<sub>60</sub>. (b) Pore radius for three stable states of MscL (closed, intermediate, and expanded) and its comparison with the pore radius for translocation of Poly(dA)<sub>60</sub>.

minimum pore radii are 0.0 Å, 2.1 and 12.5 Å for the closed, intermediate, and open states, respectively (Figure 3b). For the ssDNA translocation case, the MscL radius is between closed and intermediate states (Figure 3b). It can be inferred from the radius of ssDNA-opened MscL that this state of MscL is not stable, tending to relax to closed state. Another striking difference between ssDNA-opened and normally opened MscL is the mechanism of gating. In the normal operation of MscL, transmembrane helices M1 (Figure 1c) rotate and tilt such that they become more aligned with the plane of the membrane, and M2 helices also tilt but to a much lower degree,<sup>23,28</sup> resulting in a shortened length of MscL (Figure 3b). In the ssDNA-opened MscL, the initially closed-state length of MscL does not change, and all M1, M2, and S1 segments expand radially (Figure 3b).

An important challenge of DNA sequencing through a nanopore is to decrease the high speed of translocation. If the translocation speed can be reduced to about one base per millisecond, then single-base detection can be more easily performed in experiments. It has been shown that translocation speeds can be reduced by increasing the solvent viscosity or decreasing the temperature,<sup>2</sup> but these methods could not

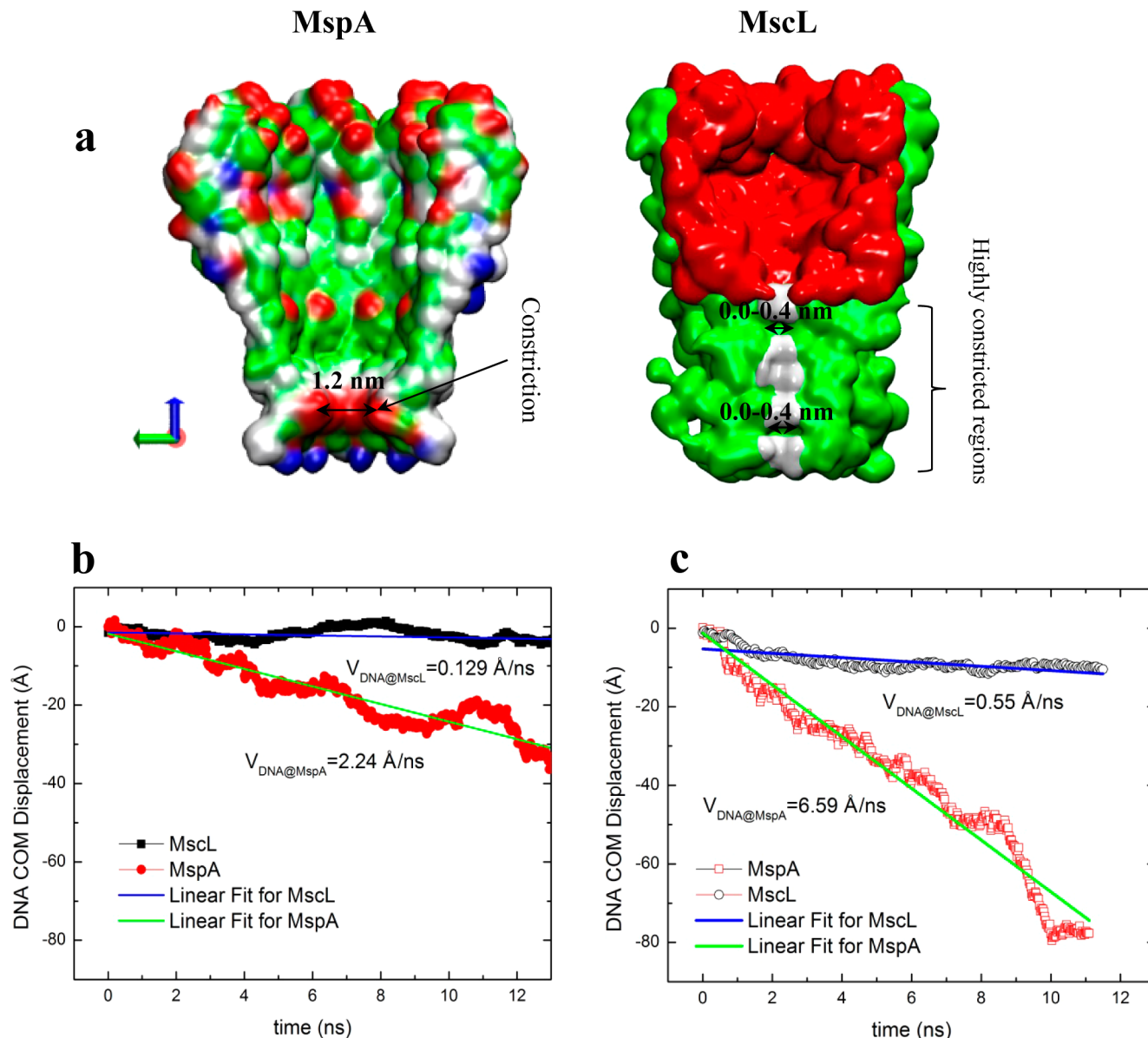


**Figure 4.** (a) Cross Sections of MspA and MscL pores and their structural differences. (b) DNA center of mass (COM) translocation history through MspA and MscL for bias = 500 mV. (c) DNA COM translocation history through MspA and MscL for bias = 1 V.

reduce the translocation speed to a desired level.<sup>2</sup> To reduce the translocation speed, an initially closed and translocation-induced elastic opening of the pore could be a potential solution. In this regard, MscL has the potential to significantly reduce the translocation speed. We compared the translocation speed of ssDNA through MscL and MspA<sup>39</sup> (Figure 4). MspA is an octameric protein with a pore suitable for DNA sequencing<sup>39,40</sup> (Figure 4a). We simulated DNA translocation keeping all conditions identical and only differing in the type of the protein. Two biases of 500 mV and 1.0 V were applied to both simulation cases to compare their speed of translocation. Translocation speed of ssDNA in MscL is 11–17 times slower than in MspA (Figure 4b and 4c). For the bias of 500 mV, the speed of translocation is 0.129 Å/ns and 2.24 Å/ns for MscL and MspA, respectively (17.36 times slower in MscL than in MspA). The reduction in speed can be attributed to two fundamental differences between these pores: (1) The comparison between MscL and MspA protein structures reveals the existence of multiple constrictions in MscL with

near zero diameters, whereas in MspA, only one constriction region with a 1.2 nm diameter is present (Figure 4a). These structural differences help reduce the speed of translocation in MscL to a large extent. (2) MspA has an open pore structure and remains roughly intact during translocation, whereas MscL opens to an extent just enough to accommodate the ssDNA bases. Since ssDNA-opened MscL does not reach an intermediate stable state, it tends to close during DNA translocation, which results in exerting force on ssDNA and reducing the speed. Based on the interaction force calculations, LYS 31, GLU 9, ARG 13, and ASP 18 residues in MscL have the highest interaction forces with ssDNA, giving rise to slower translocation of ssDNA. Interestingly, all these residues are located in constriction regions 1 and 2. It is notable that the S domain plays a critical role in the creation of highly constricted regions in MscL. The highly constricted regions in MscL give rise to the selectivity of the passage of ions for each nucleotide which increases the SNR. Also, the highly constricted regions

created by S1 domain have a significant effect on reducing the DNA translocation speed.

## CONCLUSIONS

We have shown that a mechanical signature, namely, tension in the membrane, can be effective for DNA detection through a mechanosensitive channel of large conductance, MscL. Four distinct force signals were detected for bases with forces decreasing in the order  $T > G > C > A$ . An initially closed MscL opens to ssDNA due to electric-field mediated translocation, and the pore geometry adapts to the size of each base. Ionic current signal is also distinct for each base, making the MscL pore amenable for detecting bases with two parallel signals, namely, membrane tension and ionic current. We found a completely different gating mechanism of MscL during ssDNA translocation compared to its normal operation. The translocation speed of DNA in MscL is roughly 1 order of magnitude slower compared to that in MspA.

## ASSOCIATED CONTENT

### Supporting Information

Comparison for MspA and MscL ionic current, Signal to Noise Ratio methodology, the molecular structure of DNA, and the Lennard-Jones parameters used in our simulations are described in Supporting Information. This material is available free of charge via the Internet at <http://pubs.acs.org>.

## AUTHOR INFORMATION

### Corresponding Author

\*E-mail: aluru@illinois.edu; web: <https://web.engr.illinois.edu/~aluru/>.

### Author Contributions

<sup>†</sup>(A.B.F., M.H.) These authors contributed equally to this work.

### Notes

The authors declare no competing financial interest.

## ACKNOWLEDGMENTS

This work is supported by AFOSR under Grant # FA9550-12-1-0464 and by NSF under Grants 1127480 and 1264282. The authors gratefully acknowledge the use of the parallel computing resource Blue Waters provided by the University of Illinois and National Center for Supercomputing Applications (NCSA).

## REFERENCES

- 1) Venkatesan, B. M.; Bashir, R. Nanopore Sensors for Nucleic Acid Analysis. *Nat. Nanotechnol.* **2011**, *6*, 615–624.
- 2) Branton, D.; et al. The Potential and Challenges of Nanopore Sequencing. *Nat. Biotechnol.* **2008**, *26*, 1146–1153.
- 3) Kasianowicz, J. J.; Brandin, E.; Branton, D.; Deamer, D. W. Characterization of Individual Polynucleotide Molecules Using a Membrane Channel. *Proc. Natl. Acad. Sci. U. S. A.* **1996**, *93*, 13770–13773.
- 4) Braha, O.; Walker, B.; Cheley, S.; Kasianowicz, J. J.; Song, L. Z.; Gouaux, J. E.; Bayley, H. Designed Protein Pores as Components for Biosensors. *Chem. Biol.* **1997**, *4*, 497–505.
- 5) Gu, L. Q.; Braha, O.; Conlan, S.; Cheley, S.; Bayley, H. Stochastic Sensing of Organic Analytes by a Pore-Forming Protein Containing a Molecular Adapter. *Nature* **1999**, *398*, 686–690.
- 6) Bayley, H.; Cremer, P. S. Stochastic Sensors Inspired by Biology. *Nature* **2001**, *413*, 226–230.
- 7) Clarke, J.; Wu, H. C.; Jayasinghe, L.; Patel, A.; Reid, S.; Bayley, H. Continuous Base Identification for Single-Molecule Nanopore DNA Sequencing. *Nat. Nanotechnol.* **2009**, *4*, 265–270.

- 8) Kircher, M.; Kelso, J. High-Throughput DNA Sequencing - Concepts and Limitations. *Bioessays* **2010**, *32*, 524–536.
- 9) Majd, S.; Yusko, E. C.; Billeh, Y. N.; Macrae, M. X.; Yang, J.; Mayer, M. Applications of Biological Pores in Nanomedicine, Sensing, and Nanoelectronics. *Curr. Opin. Biotechnol.* **2010**, *21*, 439–476.
- 10) Akeson, M.; Branton, D.; Kasianowicz, J. J.; Brandin, E.; Deamer, D. W. Microsecond Time-Scale Discrimination among Polycytidylc Acid, Polyadenylic Acid, and Polyuridylic Acid as Homopolymers or as Segments within Single RNA Molecules. *Biophys. J.* **1999**, *77*, 3227–3233.
- 11) Butler, T. Z.; Pavlenok, M.; Derrington, I. M.; Niederweis, M.; Gundlach, J. H. Single-Molecule DNA Detection with an Engineered MspA Protein Nanopore. *Proc. Natl. Acad. Sci. U. S. A.* **2008**, *105*, 20647–20652.
- 12) Chang, G.; Spencer, R. H.; Lee, A. T.; Barclay, M. T.; Rees, D. C. Structure of the MscL Homolog from Mycobacterium Tuberculosis: A Gated Mechanosensitive Ion Channel. *Science* **1998**, *282*, 2220–2226.
- 13) Siwy, Z. S.; Davenport, M. Nanopores Graphene Opens up to DNA. *Nat. Nanotechnol.* **2010**, *5*, 697–698.
- 14) Wells, D. B.; Belkin, M.; Comer, J.; Aksimentiev, A. Assessing Graphene Nanopores for Sequencing DNA. *Nano Lett.* **2012**, *12*, 4117–4123.
- 15) Min, S. K.; Kim, W. Y.; Cho, Y.; Kim, K. S. Fast DNA Sequencing with a Graphene-Based Nanochannel Device. *Nat. Nanotechnol.* **2011**, *6*, 162–165.
- 16) Farimani, A. B.; Min, K.; Aluru, N. R. DNA Base Detection Using a Single-Layer MoS<sub>2</sub>. *ACS Nano* **2014**, *8*, 7914–7922.
- 17) Liu, K.; Feng, J. D.; Kis, A.; Radenovic, A. Atomically Thin Molybdenum Disulfide Nanopores with High Sensitivity for DNA Trans Location. *ACS Nano* **2014**, *8*, 2504–2511.
- 18) Saha, K. K.; Drndic, M.; Nikolic, B. K. DNA Base-Specific Modulation of Microampere Transverse Edge Currents through a Metallic Graphene Nanoribbon with a Nanopore. *Nano Lett.* **2012**, *12*, 50–55.
- 19) Liu, Y. X.; Dong, X. C.; Chen, P. Biological and Chemical Sensors Based on Graphene Materials. *Chem. Soc. Rev.* **2012**, *41*, 2283–2307.
- 20) Prasongkit, J.; Grigoriev, A.; Pathak, B.; Ahuja, R.; Scheicher, R. H. Transverse Conductance of DNA Nucleotides in a Graphene Nanogap from First Principles. *Nano Lett.* **2011**, *11*, 1941–1945.
- 21) Sukharev, S.; Durell, S. R.; Guy, H. R. Structural Models of the MscL Gating Mechanism. *Biophys. J.* **2001**, *81*, 917–936.
- 22) Sukharev, S.; Betanzos, M.; Chiang, C. S.; Guy, H. R. The Gating Mechanism of the Large Mechanosensitive Channel MscL. *Nature* **2001**, *409*, 720–724.
- 23) Sukharev, S.; Anishkin, A. Mechanosensitive Channels: What Can We Learn from ‘Simple’ Model Systems? *Trends Neurosci.* **2004**, *27*, 345–351.
- 24) Jeon, J.; Voth, G. A. Gating of the Mechanosensitive Channel Protein MscL: The Interplay of Membrane and Protein. *Biophys. J.* **2008**, *94*, 3497–3511.
- 25) Sukharev, S. I.; Blount, P.; Martinac, B.; Blattner, F. R.; Kung, C. A Large-Conductance Mechanosensitive Channel in *E. coli* Encoded by MscL Alone. *Nature* **1994**, *368*, 265–268.
- 26) Perozo, E.; Cortes, D. M.; Somponpisut, P.; Kloda, A.; Martinac, B. Open Channel Structure of Mscl and the Gating Mechanism of Mechanosensitive Channels. *Nature* **2002**, *418*, 942–948.
- 27) Gullingsrud, J.; Kosztin, D.; Schulten, K. Structural Determinants of Mscl Gating Studied by Molecular Dynamics Simulations. *Biophys. J.* **2001**, *80*, 2074–2081.
- 28) Gullingsrud, J.; Schulten, K. Gating of Mscl Studied by Steered Molecular Dynamics. *Biophys. J.* **2003**, *85*, 2087–2099.
- 29) Gullingsrud, J.; Schulten, K. Lipid Bilayer Pressure Profiles and Mechanosensitive Channel Gating. *Biophys. J.* **2004**, *86*, 3496–3509.
- 30) Barriga, H. M. G.; Booth, P.; Haylock, S.; Bazin, R.; Templar, R. H.; Ces, O. Droplet Interface Bilayer Reconstitution and Activity

Measurement of the Mechanosensitive Channel of Large Conductance from *Escherichia coli*. *J. R. Soc. Interface* **2014**, *11*.

(31) Yang, L. M.; Wray, R.; Parker, J.; Wilson, D.; Duran, R. S.; Blount, P. Three Routes to Modulate the Pore Size of the MscL Channel/Nanovalve. *ACS Nano* **2012**, *6*, 1134–1141.

(32) Kale, L.; et al. NAMD2: Greater Scalability for Parallel Molecular Dynamics. *J. Comput. Phys.* **1999**, *151*, 283–312.

(33) Humphrey, W.; Dalke, A.; Schulten, K. VMD: Visual Molecular Dynamics. *J. Mol. Graph.* **1996**, *14*, 33–38.

(34) MacKerell, A. D.; Banavali, N. K. All-Atom Empirical Force Field for Nucleic Acids: II. Application to Molecular Dynamics Simulations of DNA and RNA in Solution. *J. Comput. Chem.* **2000**, *21*, 105–120.

(35) Gosse, C.; Croquette, V. Magnetic Tweezers: Micromanipulation and Force Measurement at the Molecular Level. *Biophys. J.* **2002**, *82*, 3314–3329.

(36) Monajemi, M.; Ketabi, S.; Zadeh, M. H.; Amiri, A. Simulation of DNA Bases in Water: Comparison of the Monte Carlo Algorithm with Molecular Mechanics Force Fields. *Biochem.-Moscow* **2006**, *71*, S1–S8.

(37) Dekker, C. Solid-State Nanopores. *Nat. Nanotechnol.* **2007**, *2*, 209–215.

(38) Deamer, D. W.; Branton, D. Characterization of Nucleic Acids by Nanopore Analysis. *Acc. Chem. Res.* **2002**, *35*, 817–825.

(39) Derrington, I. M.; Butler, T. Z.; Collins, M. D.; Manrao, E.; Pavlenok, M.; Niederweis, M.; Gundlach, J. H. Nanopore DNA Sequencing with MspA. *Proc. Natl. Acad. Sci. U. S. A.* **2010**, *107*, 16060–16065.

(40) Faller, M.; Niederweis, M.; Schulz, G. E. The Structure of a Mycobacterial Outer-Membrane Channel. *Science* **2004**, *303*, 1189–1192.